Engineering toughening mechanisms in architectured ceramic-based bioinspired materials

Rahimizadeh, A.; Yazdani Sarvestani, H.; Li, L.; Barroeta Robles, J.; Backman, D.; Lessard, L.; Ashrafi, B.

Publisher's version / Version de l'éditeur:
https://doi.org/10.1016/j.matdes.2020.109375
Materials & Design, 198, pp. 1-12, 2021-01-15

Materials and Design 198 (2021) 109375

Contents lists available at ScienceDirect

Materials and Design

journal homepage: www.elsevier.com/locate/matdes

Engineering toughening mechanisms in architectured ceramic-based bioinspired materials

A. Rahimizadeh [a,b], H. Yazdani Sarvestani [a,*], L. Li [c], J. Barroeta Robles [a], D. Backman [c], L. Lessard [b], B. Ashrafi [a,*]

[a] Aerospace Manufacturing Technology Center, National Research Council Canada, Montreal, QC H3T 2B2, Canada
[b] Department of Mechanical Engineering, McGill University, Montreal, QC H3A0C3, Canada
[c] Structures and Materials Performance Laboratory, National Research Council Canada, Ottawa, ON K1A 0R6, Canada

HIGHLIGHTS

- Developing a comprehensive model to design a new class of architectured ceramics.
- Developing industrially scalable fabrication technique based on a laser system.
- Exploring dynamic toughening mechanisms of bioinspired ceramics.
- The primary toughening mechanisms is extensive crack deflection and delamination.

GRAPHICAL ABSTRACT

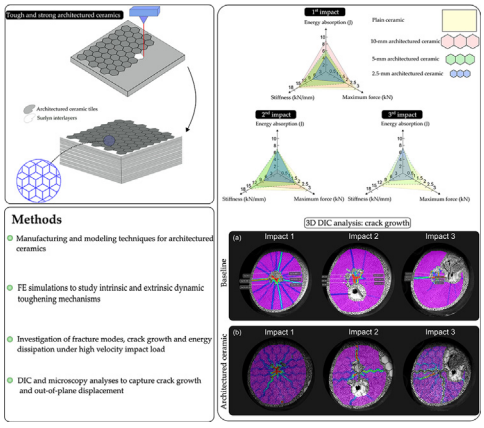

ARTICLE INFO

Article history:
Received 16 September 2020
Received in revised form 28 November 2020
Accepted 30 November 2020
Available online 2 December 2020

Keywords:
Bioinspired materials
Architectured ceramics
Computational model
Digital image correlation
Dynamic toughening mechanisms

ABSTRACT

Ceramics offer many attractive properties including low-density, high compressive strength, remarkable thermal stability, and high oxidation/corrosion resistance. However, these materials suffer from brittleness, which substantially limits the range of their applications, where high toughness is required. This investigation draws inspiration from a concept of architectures with three-dimensional (3D) networks of weak interfaces targeting high toughness ceramics. In this study, a comprehensive method combining an advanced computational model with 3D digital image correlation (DIC) was developed to engineer bioinspired multilayered architectured ceramics and assesses their toughening and deformation mechanisms when subjected to a low-velocity impact load regime. A complete finite element (FE) analysis was conducted to precisely evaluate the crack growth and displacement field of the architectured ceramics and is compared to those of plain ceramics. The damage and displacement evolution results from FE analysis and experimental testing revealed that the primary source of toughening of the architectured ceramic systems is extrinsic, resulting from extensive crack deflection and delamination. Crack propagation along an irregular long path at the weak interfaces of architectured layers increased the toughness of the plain ceramics by two orders of magnitude. Based on the DIC data, both extrinsic and intrinsic toughening mechanisms were captured: sliding of the tiles in the architectured ceramics and channel plastic deformation in adhesive interlayers, respectively.

* Corresponding authors.
E-mail addresses: hamidreza.yazdani@nrc-cnrc.gc.ca (H. Yazdani Sarvestani), behnam.ashrafi@nrc-cnrc.gc.ca (B. Ashrafi).

https://doi.org/10.1016/j.matdes.2020.109375

1. Introduction

The capability to engineer a material's architecture provides an avenue to reach superior mechanical, electrical, chemical, and thermal properties. New design approaches and novel manufacturing methods are required to control and tune architectures over multiple length scales [1]. These concepts are to be exploited to generate high performance ceramic systems used in extreme thermo-mechanical conditions such as thermal protection systems in gas-turbine engines, leading edges, or nozzle engine components. Attributes such as low-density and high compressive strength combined with excellent thermal stability, and high oxidation and corrosion resistance make ceramics an excellent candidate to be used in these extreme environments. However due to the low fracture toughness and damage tolerance of this material, challenges arise that prevent widespread use of the material's strategic application in aerospace, marine, automotive, armour and power-generation industries [2,3]. Fig. 1 presents the Ashby materials chart [4] outlining the fracture toughness and Young's modulus of the common materials used in these industries. As observed in Fig. 1, there are currently no existing technical ceramics that can provide a combination of high stiffness and fracture toughness.

Several strategies have been developed to enhance the mechanical properties of ceramics such as nanomaterial dispersion, minimizing grain size and porosity, and microstructure control, reduction of crystal anisotropy and localized stresses, and functionally grading glass/ceramic/glass structures. Laminating or pre-stressing ceramics can also improve their damage tolerance, but the impact resistance and toughness have not been significantly improved [3]. These strategies have been observed and applied only at small, laboratory scales. However, large-scale, and viable manufacturing technologies are still a bottleneck for industrial applications. Recently, novel approaches inspired by natural materials such as bone, teeth and mollusk shells have been developed to overcome the inherent brittleness of ceramics [5–7]. These bioinspired approaches use exceptional toughening tactics to design and program multifunctional ceramic-based materials featuring tuneable strength, toughness, and excellent thermal and electrical properties [8].

Architectured materials represent another type of bioinspired materials (such as the structure of fish fins, spines and tesserae in shark skeletons [9,10]), which offer damage confinement, crack deflection and delamination, and which delay or arrest damage due to crack propagation and thus toughness improvement [6,11,12]. Architectured materials have successfully served as the concept and inspiration to design novel materials built from brittle components (such as ceramics and glasses) with high energy absorption capability [13–15]. These materials are arranged in layers, alternating between hard architectured building blocks, and a softer interface to which it is bonded. The geometry and properties of the hard building blocks combined with the properties of softer interface can allow for large nonlinear deformations resulting in a combination of stiffness, strength and toughness [6,7]. Therefore, the architectured materials designed with a network of weak interfaces can harness powerful inelastic mechanisms including frictional sliding, delamination and fracture energy dissipation leading to structures that can be up to three orders of magnitude tougher than their brittle constituents [16]. The structural toughening mechanisms can be classified as either intrinsic or extrinsic [17]. Intrinsic mechanisms act ahead of the crack tip, are independent from the crack size or geometry, and commonly arise from the effects of plasticity. In contrast, extrinsic toughening includes microstructural mechanisms that act behind the crack tip. The extrinsic mechanisms result from frictional sliding or interlocking between two rough fracture surfaces in the case of multilayered structures. Both intrinsic and extrinsic toughening mechanisms have been studied in a variety of structures including ceramic composites [18,19], natural materials such as bamboo [20,21], and biological materials such as mollusk shells and bone [22,23]. Despite the recent efforts designing and manufacturing architectured ceramics [24–26], less attention has been paid to exploring the dynamic toughening and deformation mechanisms of the architectured ceramic-based bioinspired materials using both computational and experimental methods.

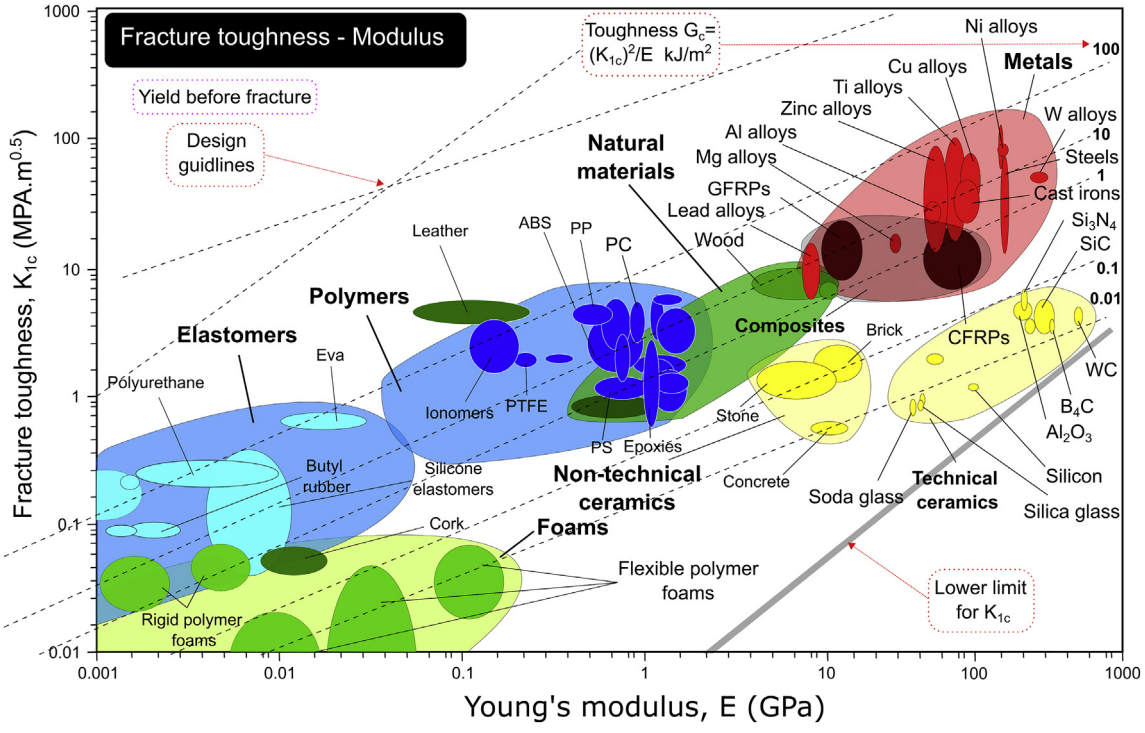

Fig. 1. Materials chart: fracture toughness vs. Young's modulus: two mechanical properties that tend to be mutually exclusive (chart is based on similar charts by Ashby).

The focus of this study is to engineer the crack path in ceramic-based bioinspired materials through architectures featuring 3D networks of hexagonal building blocks with weak interfaces. The role of various toughening and deformation mechanisms in their hexagonal architectures is then studied to shed light into the toughening mechanisms of natural materials. The developed model combines a computational analysis using ABAQUS and 3D digital image correlation (DIC) to assess these mechanisms. These analyses provide insights into the displacement field and the structure-mechanics-performance relationship of the architectured bioinspired ceramic systems under a low-velocity impact load. Dynamic explicit analysis in ABAQUS has been carried out to find the force-displacement response, energy dissipation as well as damage growth in the plain and architectured ceramics. The developed model will enable the ceramic and glass industrial communities to achieve superior material performance (i.e., high strength, toughness and multi-impact resistant) by using a promising manufacturing method involving three-dimensional laser cutting and lamination system [7,27,28].

2. Materials and methods

Concepts of natural materials were used to develop novel multilayered ceramics featuring a hexagonal architecture and reframed their mechanical performance as a relationship between the size of a hexagonal building block and a soft interfacial polymer. These concepts are first applied to achieve multilayered ceramics featuring a soft interface. Then, the energy absorption of the structure is evaluated to gain insight into the complex dynamic toughening mechanisms that underpin the damage dissipation featured in natural materials with similar architectures.

2.1. Design and manufacturing

To engineer the laser-engraved architectured ceramics and to determine their energy absorption and multi-hit capabilities, an experimental set-up was assembled as shown in Fig. 2. The main components of this setup include a laser engraver (Model YLR-5000, IPG Photonics Corporation, Oxford, MA, USA) which can generate 100% cutting depth on ceramic sheets along a set of predefined focal points [17], a vacuum bagging system to firmly bond adhesive interlayers and ceramic tiles, and a high speed 3D DIC tests system to assess the displacement field due to impact loading on the samples.

First, a continuous UV laser (1070 nm, 5 kW cw pumped, 50 kHz repetition rate, 80 μs pulse duration) was used along the edges of predefined hexagonal building blocks to cut architectured tiles on 635 μm thick, square, optical grade 263 M borosilicate ceramic sheets (high-tolerance non-porous alumina ceramic with 96–99.8% material composition, McMaster-Carr, No. 8462 K2). This process is depicted in Fig. 2a. Next, Surlyn® thermoplastic, which has been shown to resemble biopolymers [29], was used as a soft polymer interface between the architectured ceramic tiles in order to mimic the crack deflection mechanisms of nacre. Some aspects of these crack deflection mechanisms include the strong adhesion to ceramic tiles, large shear deformation, as well as the viscous properties of Surlyn® which provide a suitable elastomeric response, which can in turn delay localized interfacial fractures. As a result, 8-layer architectured ceramics were laminated with thin Surlyn® films at the interface, as shown in Fig. 2b. The entire panel was then placed in an oven and maintained at 146 °C for 5 h to partially melt the adhesive and to attain a prefer bonding between the layers. This process was performed under vacuum as shown in Fig. 2c. The protocol above was

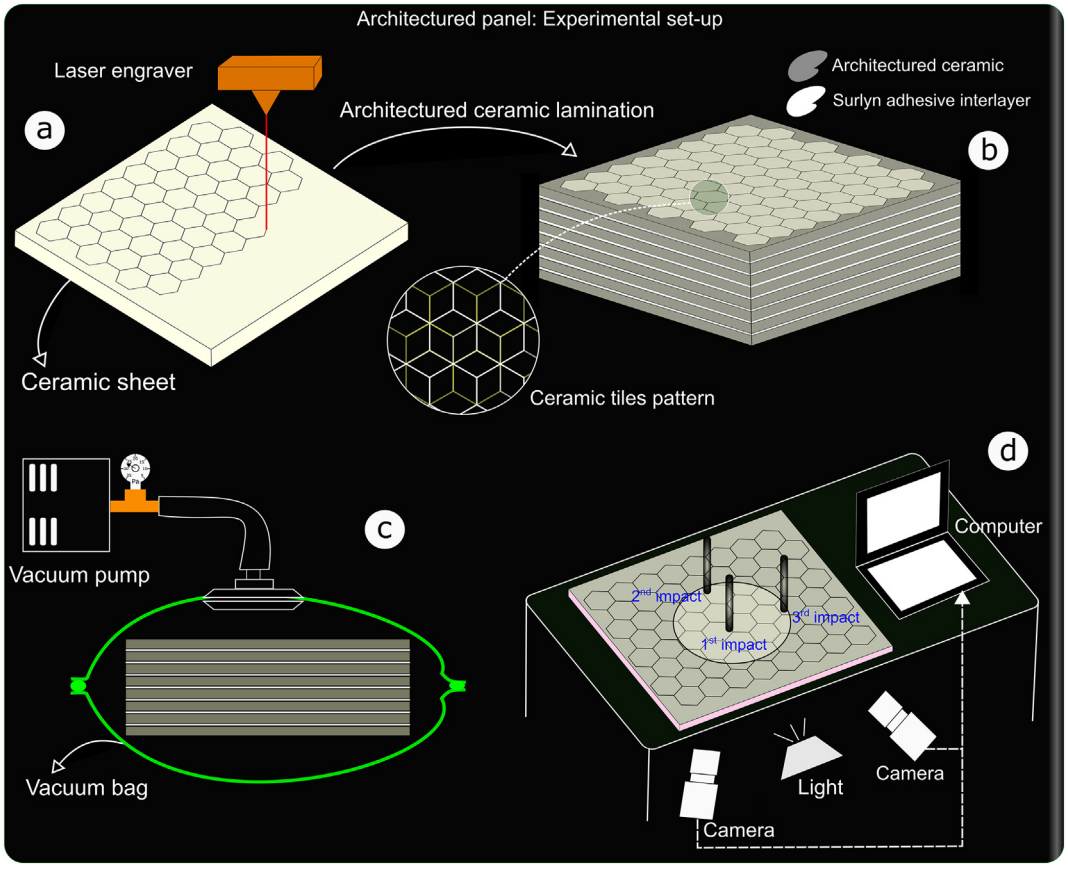

Fig. 2. Taxonomy of the experimental set-up: (a) Creation of ceramic building blocks via laser cutting ceramic system, (b) Laminating ceramic tiles with Surlyn film®, (c) Vacuuming the architectured ceramics to ensure perfect bonding at the interface, and (d) Low-velocity impact testing with 3D DIC analysis through a mirrored reflections of the actual test.

followed to manufacture three different designs with ceramic tiles of 2.5, 5, and 10 mm for side lengths of hexagons. As a baseline, a plain ceramic was also manufactured through the same fabrication process for comparison purposes.

The energy dissipation response and the toughening mechanisms of the architectured ceramics were studied under three consecutive low-velocity impacts. As per ASTM D3763 [30], using a spherical impactor with a diameter of 5 mm and weight of 12 kg. The effect of resistance loads from the support was minimized by putting the samples on a fixture with a central hole of 76.2 mm in diameter. During the test, the impactor load and velocity were measured to obtain the load displacement curves. The former was measured through a penetration piezoelectric load sensor with a load capacity of 22.5 kN, and the latter was captured using a photo detector block and a flag. The setup is depicted in Fig. 2d.

2.2. Digital image correlation

A 3D DIC system was used during the low-velocity impact tests to measure the deformation of the bottom surface of the ceramics (see Fig. 2d). The stereoscopic DIC system consisted of two high-speed cameras (Photron SA-X) set to capture images at 20,000 frames per second (fps) with a resolution of 1024 × 632 pixels. A first surface mirror was placed below the drop tower table and the undersurface of the ceramic sample was imaged through the mirror. Extra lighting was provided to reduce the exposure time sufficiently, thus enabling 20,000 fps image capturing rate. In addition, a stochastic speckle pattern was applied to the bottom surface of the ceramic using black coloured sharpies. DIC data were analyzed using the VIC3D software (version 8, Correlated Solutions Inc.).

As an optical method, the DIC algorithm subdivides an area of interest in the reference image, in this case the image of speckle pattern on the ceramic surface captured prior to beginning of the test, into regularized square regions denoted as subsets. The methodology then allocates a shape function to each of the subsets, and using cross-correlation algorithm, the deformed configurations of each subset are identified in the (deformed) images of the speckled surface captured during testing. Through determining the correspondence between each of the deformed and reference subsets the full field displacement over the area of the interest can be calculated and then later differentiated to produce a full field strain map for each of the test images.

The shape matching nature of the DIC algorithm necessitates rigorous subset and speckle size requirements. In general, the subset size should be large enough to contain distinctive speckle features to ensure the uniqueness of the subset and avoid data loss during the correlation calculation, but also small enough to satisfy geometrical constraints on the specimen's surface as well as preventing significant reduction in spatial resolution and impractical algorithm runtime. The cross-correlation metric applied during subset matching stage operates directly on the grayscale values of the images, thus it is important to optimize the contrast between the speckle color and the associated background shading. This serves to improve the confidence and accuracy for the cross-correlation results. In this test, the ceramic tile provided a natural white coloured background, hence the maximum grayscale contrast can be achieved using black coloured sharpies.

DIC analysis on the low-velocity impact test images resulted in spatially and temporally dense full field displacement and strain data maps. The displacement data was then available for both qualitative comparison with the FE analysis results as well as more quantitative validation. However, due to significant crack nucleation and propagation throughout the area of interest during the tests, the strain data maps experience artifacts along and around the crack path as the cracked region results in fictitious strain. Thus, the strain data were only used for qualitative purposes to capture the failure initiation and propagation throughout the specimens, while the displacement data was used for quantitative comparisons and analysis.

2.3. 3D laser scanning microscopy

Following impact testing, the damaged surface of the ceramics was precisely investigated via confocal laser scanning microscopy (VK-X200) to image the crack growth within the layers. Microstructural crack paths and deflections, as well as delamination, were observed on the fracture planes and the top surface of the specimens.

2.4. Finite element modeling

To aid in the investigation and engineering of the energy absorption of the architectured ceramics described above, a set of FE simulations (ABAQUS/EXPLICIT) was performed in parallel to the experimental work detailed above. The complimentary results on one hand were used to validate the FE model and on the other hand, they served to precisely capture the mechanisms that govern the energy absorption of the ceramics subjected to a low velocity impact load, thus aiding to further the design of a new class of architectured ceramics.

For the ceramic material, the Johnson-Holmquist (JH-2) [31] constitutive response model was used to obtain the evolution of damage inside the ceramics subjected to large strain rates imposed by dynamic impact loading. The JH-2 model uses normalized strength parameters with respect to Hugoniot Elastic Limit (HEL) to allow for a more precise modeling of impact response. Damage in the JH-2 model is represented via a state variable, which corresponds to the average damage within a specific finite volume of the material such that the evolution of damage is associated with strength reduction. In particular, the equivalent stress (σ^*) inside the ceramics can be determined in terms of the damage parameter, D, as:

$$\sigma^* = \sigma_i^* - D\left(\sigma_i^* - \sigma_f^*\right) \tag{1}$$

where σ_i^* and σ_f^* denote the normalized intact and fracture strength, respectively. A damage parameter of 0 indicates an intact material, whereas a fully fractured material features a damage parameter of 1. The intact material strength is given by:

$$\sigma_i^* = A\,(P^* + T^*)^N(1 + \mathrm{C}\ \ln\varepsilon^*) \tag{2}$$

where A is the intact strength parameter, P^* is the normalized pressure, T^* represents the normalized maximum tensile strength, N is the material constant, C is the strength constant for strain rate dependence, and ε^* is the strain rate. All the strength parameters are normalized with respect to the HEL. The fracture strength can be defined as:

$$\sigma_f^* = B\,(P^*)^M(1 + \mathrm{C}\ \ln\varepsilon^*) \tag{3}$$

where B is the fracture strength parameter, and M is the material constant. The equation of state for a brittle material under dynamic loading can be written in terms of excess compression as:

$$P = K_1\mu + K_2\mu^2 + K_3\mu^3 + \Delta P \tag{4}$$

where $\mu = \frac{\rho}{\rho_0} - 1$, and ρ_0, ρ are the initial and final densities, respectively. In addition, K_1, K_2 and K_3 are constants obtained from plate impact or diamond anvil press experiments. All the coefficients adopted in the FE analysis are reported in Table 1 and were obtained from previous measurements [32].

The Surlyn adhesive interlayers were modeled using cohesive elements with traction-separation behaviour. The maximum traction of cohesive failure was set to 3.2 MPa and the elastic constants were calculated from the shear and Young's modulus of Surlyn [29]. A mixed mode Benzeggagh-Kenane (BK) fracture criterion with a coefficient of 1.45 and linear softening behaviour was used for damage evolution. The proper selection of these values is critical as they can impact the fracture mode of the ceramic at the interface. Therefore, the cohesive traction

Table 1
JH-2 properties used for FE analysis of ceramics.

Material properties	Alumina	Material properties	Alumina
ρ (Density (kg/m^3))	3850	Hugoniot elastic limit (GPa)	8
G (Shear modulus (GPa))	123	pHEL (HEL pressure (GPa))	1.46
A (normalized intact strength coefficient)	0.949	THEL (HEL strength (GPa))	2.0
B (normalized fractured strength coefficient)	0.1	D_1 (Damage constant)	0.001
C (strain rate constant)	0.007	D_2 (Damage constant)	1.0
M (fractured strength exponent)	0.2	β (Bulking factor)	1.0
N (intact strength exponent)	0.2	K_1 (Pressure constant (GPa))	186.8
T^* (Tensile strength (GPa))	0.262	K_2 (Pressure constant (GPa))	0
SF_{max} (Normalized fracture strength)	1e20	K_3 (Pressure constant (GPa))	0

was taken from the results of a shear lap test and the fracture energy was accordingly tuned to precisely reproduce the experimental response of the plain ceramic.

Fig. 3 illustrates the steps that were followed to create the solid model of the architectured ceramics. As seen, a ceramic hexagonal tile featuring a thickness of 635 μm and three different side lengths including 2.5, 5 and 10 mm were first created and patterned to generate the ceramic ply with the dimension of 100 × 100 mm^2 (see Fig. 3a). A dynamic frictional contact with a coefficient of 0.36 was imposed between the tiles to represent the 100% laser cut depth. The adhesive interlayers were created with a thickness one order of magnitude thinner than that of the ceramic tiles. As depicted in Fig. 3b, the ceramic tiles and adhesive interlayers were then stacked together with a tie constraint at the interfaces between adjacent plies to prevent interpenetration. The spherical impactor with a diameter of 5 mm and weight of 12 kg was modeled as an analytically rigid part with an initial velocity of 2.1 m/s. The architectured ceramic was then placed on a rigid support with a middle circular hole featuring a diameter of 76.2 mm. A general contact formulation with frictionless property was defined between the support, impactor, and the ceramic panel. The parameters of the JH-2 and traction-separation models were then inputted based on the response curves shown in Fig. 3c and d.

Both the ceramic tiles and adhesive interlayers were meshed with structured hexahedral elements. For the former, linear 3D stress elements (C3D8R) with reduced integration were used, and for the latter, the linear cohesive element (COH3D8) was adopted. The adhesive interlayers were selected as slave contact surfaces and the accuracy of the results was enhanced using a finer mesh for the adhesive interlayers relative to the ceramic tiles. Mesh convergence analysis was performed to determine whether enough elements had been included for each analysis.

3. Results

In this section, the force-displacement response, stiffness, and energy absorption capability (the area under the force-displacement curve) of the developed architectured ceramics are discussed. These results reveal the underlying toughening mechanisms that lead to the distinct characteristics of these structures when compared with plain ceramics. A set of experimental and computational results from three consecutive impacts is described.

Figs. 4 and 5 show the out-of-plane displacement field of the plain ceramic and 5-mm hexagonal architectured ceramic obtained via 3D DIC analysis on the bottom surface of the panel, opposite of the impact

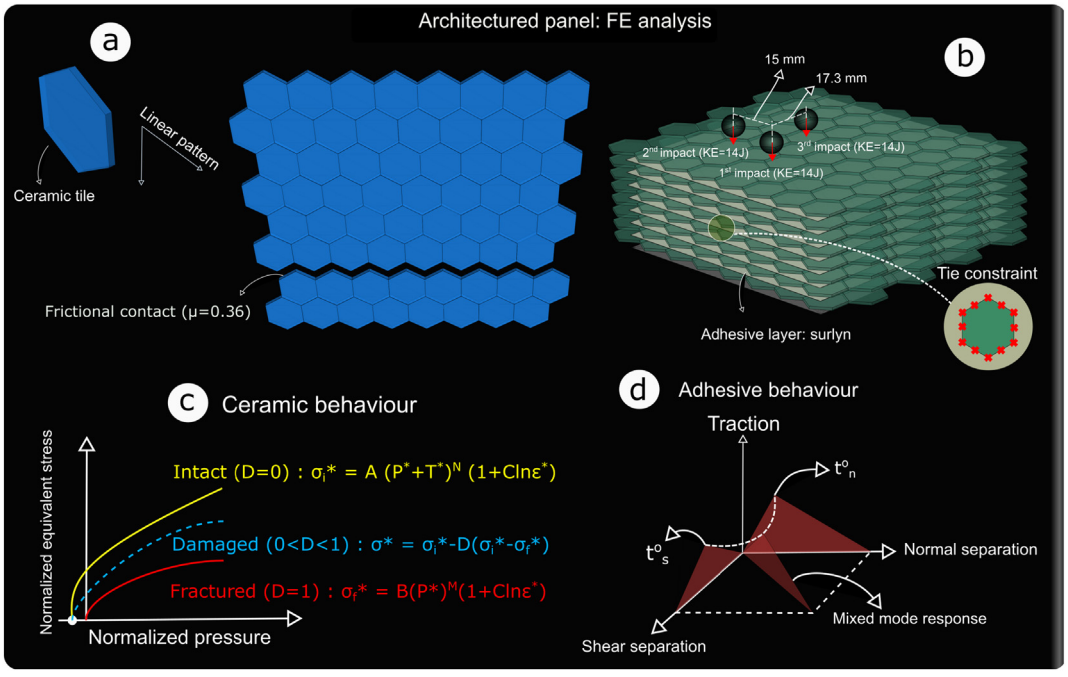

Fig. 3. Schematic showing the FE analysis: (a) Generation of architectured ceramic ply, (b) Assembly of the parts and definition of contact formulations, (c) Mechanical behaviour of ceramic tiles, and (d) Mechanical behaviour of adhesive interlayers.

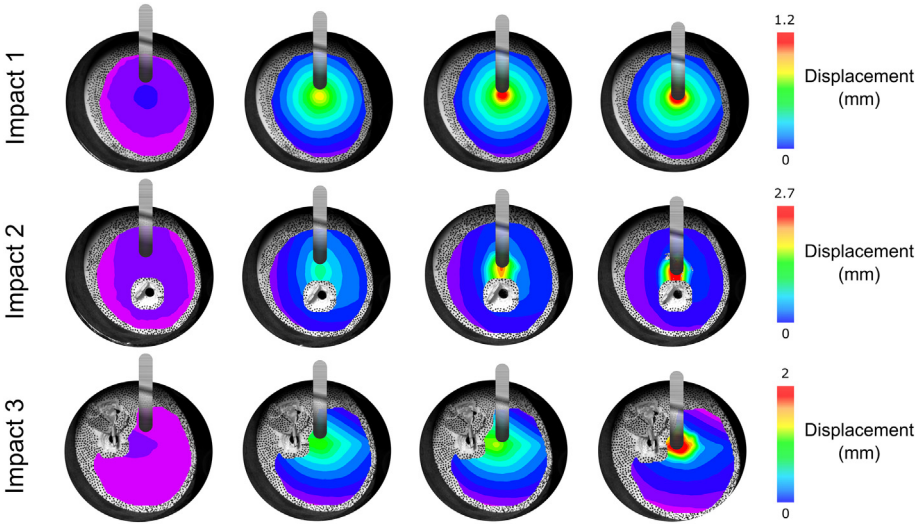

Fig. 4. Impact displacement distribution on the bottom layer of the plain ceramic measured experimentally.

surface. The results demonstrated that the displacement in the architectured ceramic is distributed more evenly throughout all three impacts as opposed to the plain one, in which the displacement map is more concentrated near the impact site. Following the first impact, an area of 7×7 mm^2 on the plain ceramic undergoes an out-of-plane displacement of 1.2 mm. On the other hand, an area of 20×20 mm^2 on the architectured ceramic (with 16 hexagonal tiles) contribute to a similar impact displacement, an extrinsic phenomenon that can lower the probability of severe localized damage, as well as the local stress and strain gradient.

Fig. 6 illustrates a comparative study between the force-displacement curves obtained via experimental impact testing and numerical analysis. The jagged impact response of ceramics indicates the initiation and propagation of microcracks. The experimental energy dissipation measured from the change in the kinetic energy of the impactor is also compared with the different toughening mechanisms observed during the FE analysis. It should be noted that following the first and second impacts, the 10-mm hexagonal architectured ceramic experienced severe damage such that its force-displacement response could not be precisely captured for the third impact. The toughening mechanisms captured from FE includes frictional dissipation that mainly results from frictional contact between the tiles; internal energy that combines elastic recoverable energy stored in the tiles and damage dissipation energy; and viscous damping that arises from the adhesive interlayers, which resist against vertical indentation of the impactor.

As seen in Fig. 6, both the FE and experimental results showed a similar trend with a good quantitative agreement. The impact response of all the samples was associated with the formation of microcracks, which propagated throughout the parts with different configurations resulting in different toughnesses. In particular, the architectured ceramics showed a significantly higher toughness relative to the plain one (i.e., baseline). This enhanced toughness can be mainly attributed to the larger inter-tile frictional dissipation of the architectured ceramics such that the 10-mm hexagonal ceramic, as shown in Fig. 6b, showed an average frictional dissipation one order of magnitude larger than that of the baseline (see Fig. 6a). The fully separated hexagons undergo micro sliding in various directions at the interface turning the impact energy into thermal energy, an extrinsic toughening mechanism that is enhanced by increasing the number of tiles in each layer. For instance, decreasing the side length of hexagons from 10 mm to 5 mm led to an increase of 80% in the frictional energy dissipation, thus generating a tougher structure. Similar pattern was also observed for the 5-mm and

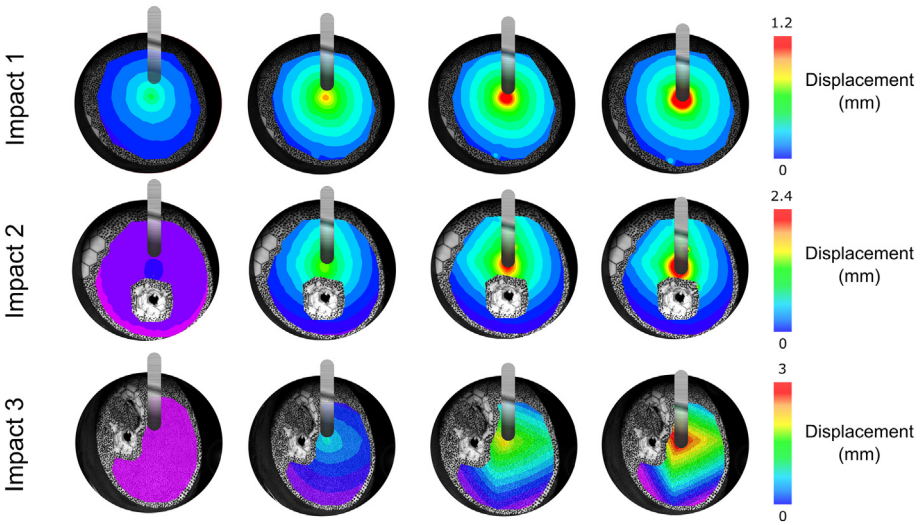

Fig. 5. Impact displacement distribution on the bottom layer of the 5-mm hexagonal architectured ceramic measured experimentally.

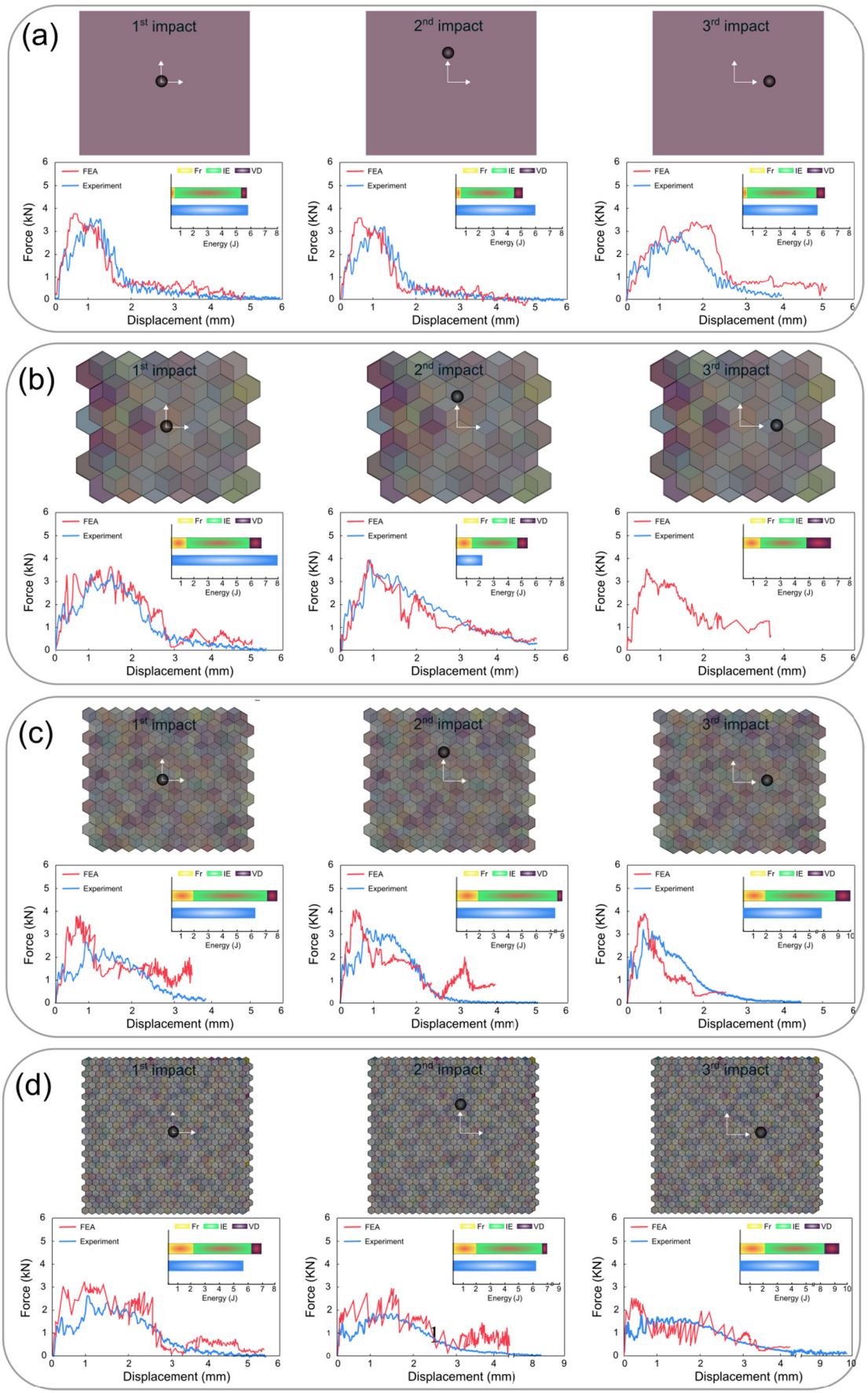

Fig. 6. Force-displacement curve and energy dissipation of ceramics: (a) Plain ceramic; (b) 10-mm hexagonal ceramic; and (c) 5-mm hexagonal ceramic; (d) 2.5-mm hexagonal ceramic. (Fr: Frictional dissipation, IE: internal energy, VD: viscous dissipation).

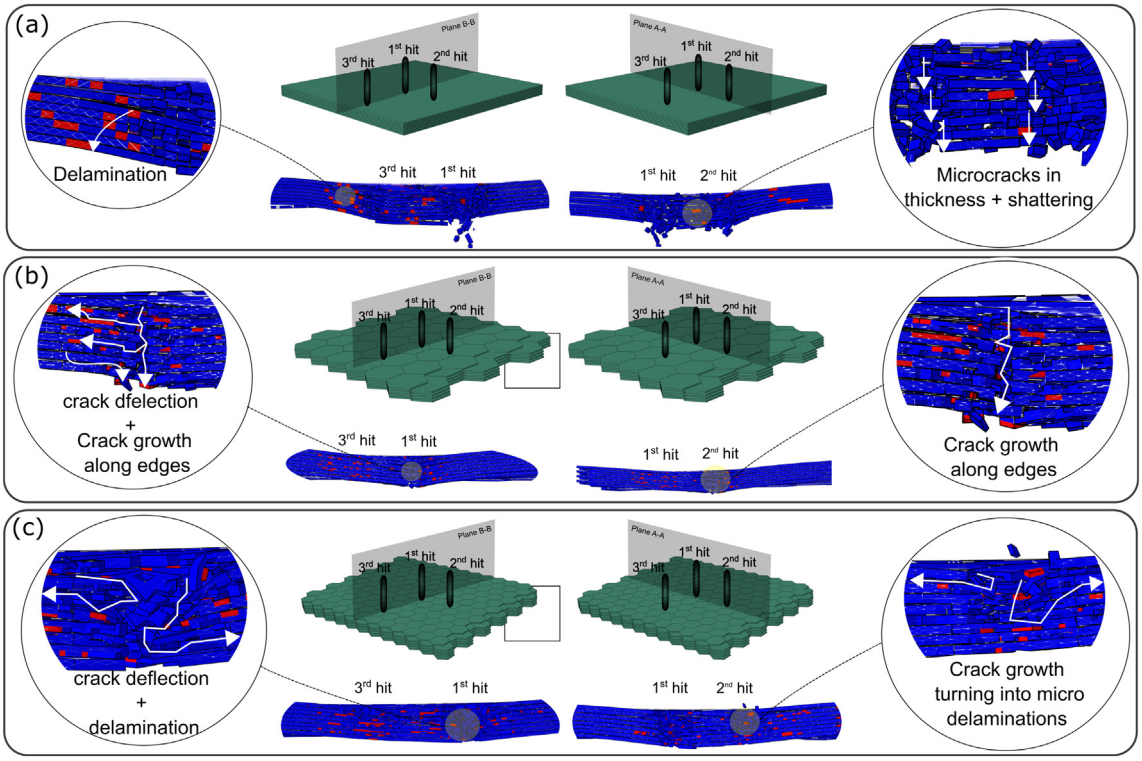

Fig. 7. Through the thickness crack propagation: (a) Plain ceramic, (b) 10-mm hexagonal ceramic, and (c) 5-mm hexagonal ceramic.

2.5-mm hexagonal ceramics, as shown in Fig. 6c and d. In addition to frictional dissipation as an extrinsic toughening mechanism, the irregular crack path throughout the thickness of the architectured ceramics can be another critical factor contributing to their better energy absorption capability. Fig. 7 presents the through-the-thickness damage growth of the ceramics along two fracture planes, namely planes A-A and B-B, where the former represents the fracture plane of the first and second impacts, whereas the latter shows the damage growth of the first and third impacts. FE results for the baseline demonstrated the formation of small straight flexural cracks through the thickness of the layers following the first impact. These flexural cracks were mainly located towards the bottom of the ceramic, which caused severe element fracture and shattering. Following the third impact, some delamination between the layers located near the outer edges of the ceramic was also observed, which resulted from adhesive debonding. In contrast, the architectured ceramics showed an irregular crooked crack path following all the impacts. In particular, the cracks mostly propagated along the cut edges of the hexagons, a damage pattern that was associated with crack deflection through excessive shear deformation of adhesive. The crack deflection zones in the adhesive interlayers resulted in numerous layer debonding, which further increased the crack path and prevented a catastrophic brittle failure.

To further highlight the increased energy absorption and multi-hit capabilities of the architectured ceramics, their coefficient of restitution (COR) was calculated by using the initial and final velocity of the impactor obtained via FE analysis. The COR measure indicates the amount of conserved kinetic energy in the impactor after it bounces off the ceramic surface. The results, as shown in Fig. 8, demonstrated that for an impact energy of 14 J, the architectured ceramics can lead to lower COR by dissipating a larger amount of kinetic energy. For instance, the 5-mm hexagonal ceramic showed a COR value reduced by, respectively, 18%, 20% and 28% after the first, second and third impacts compared to the

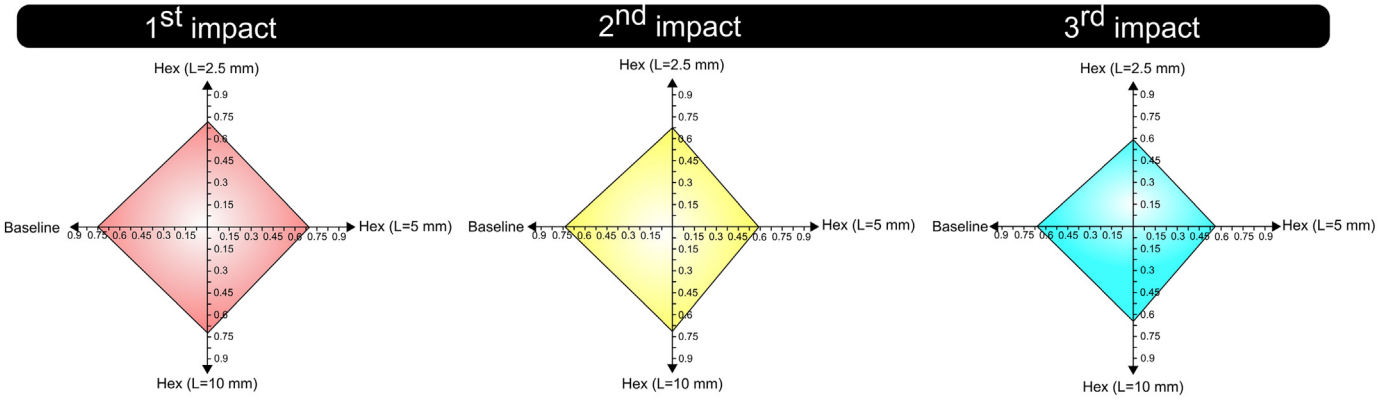

Fig. 8. The coefficient of restitution for the impactor following all three consecutive impacts. The smaller values calculated for architectured ceramics demonstrate their enhanced energy dissipation.

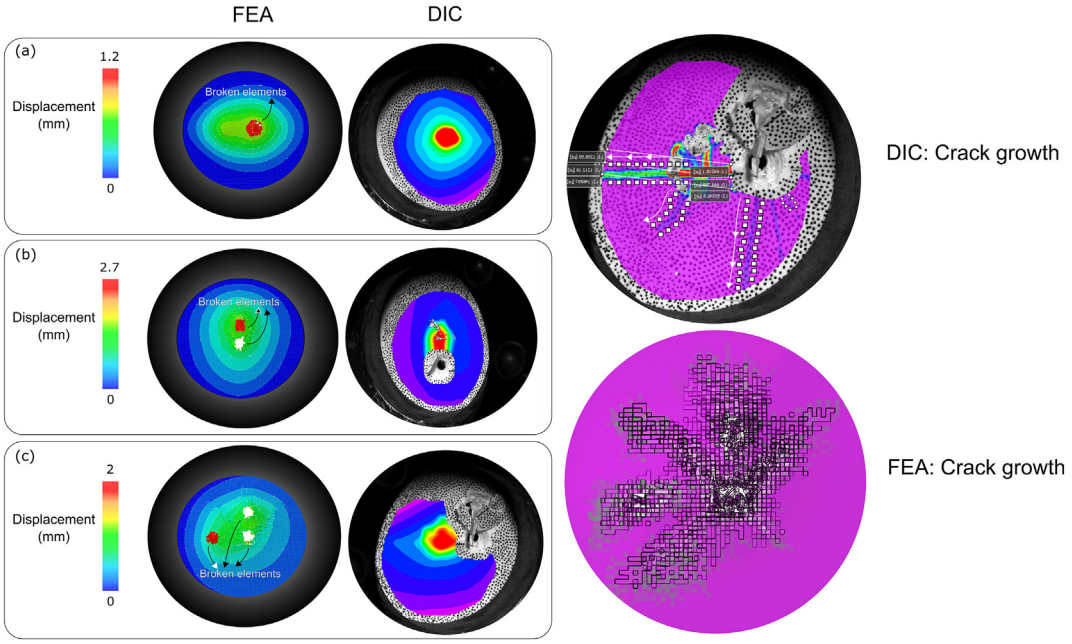

Fig. 9. Comparison of displacement evolution and in-plane crack growth of the plain ceramic obtained via DIC and FE analysis: (a) First impact; (b) Second impact; (c) Third impact.

corresponding COR value of the baseline. These results indicate that a more complex energy dissipation system composed of different mechanisms contributed to the conservation of energy in the impactor after it collides with the architectured ceramics, thus any change in the initial velocity of the impactor can lead to different COR value.

DIC analysis provided further guidance in assessing the role of crack deflection in toughening mechanisms of ceramics. Figs. 9 and 10 present the comparison between 3D DIC and FE data maps displaying the displacement distribution and in-plane crack growth of the baseline and 5-mm hexagonal architectured ceramic. Following the first impact on the baseline, several cracks were formed around the impact site and rapidly propagated to the outer edges. The crack initiation occurred at a deflection of approximately 0.1 mm during the first impact. The same pattern was also observed after the second and third impacts such that several microcracks were formed and grown in an irregular path. Unlike the plain ceramic, the architectured ones did not show any localized fracture and the majority of cracks were mainly oriented to the edges of the hexagons, an observation that can be attributed to the crack deflection phenomenon that occurred at the interface between the hexagonal tiles and Surlyn® interlayers. The initial cracks were observed at a deflection of 0.3 mm, which is approximately twice the displacement when comparing to the baseline. The plastic

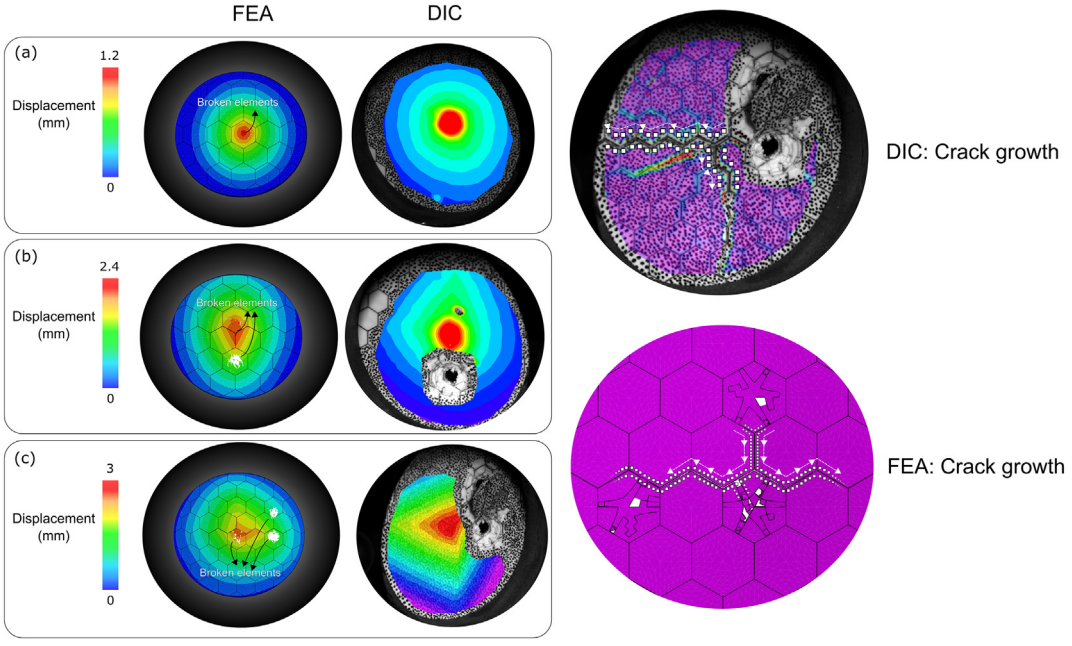

Fig. 10. Comparison of displacement evolution and in-plane crack growth of the 5-mm hexagonal ceramic obtained via DIC and FE analysis: (a) First impact; (b) Second impact; (c) Third impact.

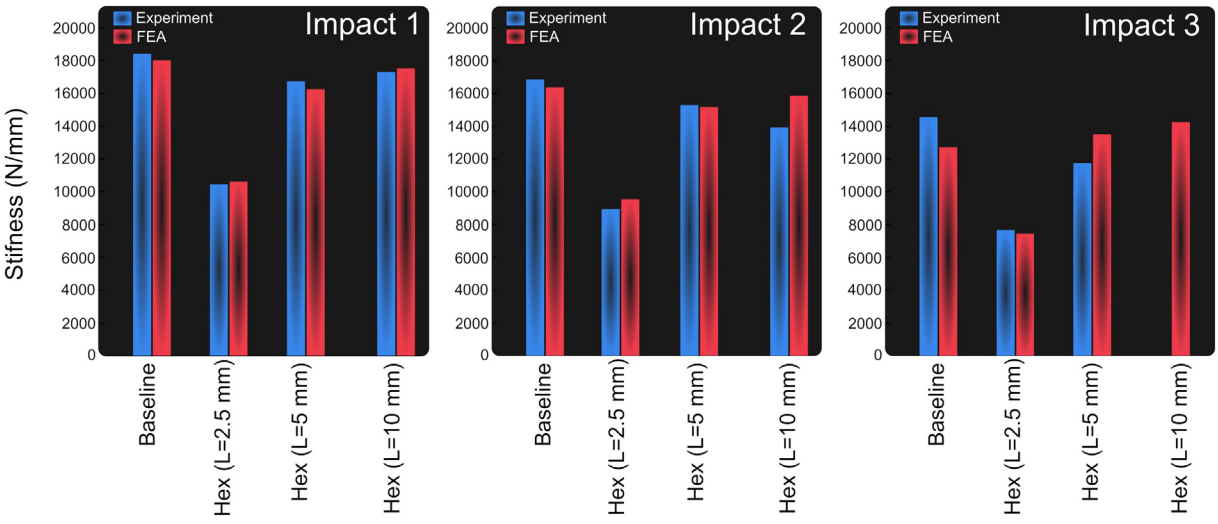

Fig. 11. Impact stiffness of the multilayered plain and architectured ceramics following three consecutive low velocity impacts obtained from velocity data captured using a photo detector and a flag.

deformation of the adhesive interlayers due to shear loads blocked the cracks from propagating to the bottom of the panel and they were deflected to the edges, a phenomenon that was associated with transverse sliding of the tiles and thus minor delamination throughout the samples.

The average initial slope of the force-displacement curves was used to evaluate the stiffness of the ceramics. The slope between the peak and subsequent arrest points (where cracks stopped), are calculated until the maximum force is reached and the average value is reported as the stiffness. The FE results validating the experimental measurements are shown in Fig. 11. Due to the complete fracture of the 10-mm hexagonal architectured ceramic after the second impact, its stiffness is not shown. As expected, the architectured ceramics featured a lower stiffness when compared with the baseline, a discrepancy that evolved by reducing the hexagon size. In addition, all the ceramics showed reduced stiffness when comparing between the first and the last impacts. Nevertheless, the reasonable retention of stiffness in the architectured ceramics following the second and third impacts elucidate that the frictional joint of hexagons in their 3D network architectures has no substantial negative influence in their multi-hit capability.

4. Discussion

Fig. 12 illustrates the impact response of the multilayered ceramics including experimental maximum force, stiffness, and energy absorption performance. There are several intrinsic and extrinsic mechanisms that play a role in the dynamic energy dissipation of the architectured and plain ceramics. For instance, the enhanced toughness of the developed multilayered architectured ceramics lies in both intrinsic and extrinsic mechanisms. However, the main source of toughness in the architectured ceramics is extrinsic. Based on the FE modeling and DIC techniques, some of these mechanisms include plastic deformation in the adhesive interlayers, frictional tile sliding, debonding between the adhesive and the ceramic tiles, crack deflection (i.e., twist), process zone and ceramic fracture. The extrinsic toughening mechanisms such as frictional tile sliding, arises from weak interfaces as potential location for cracks to initiate and propagate (unlike intrinsic mechanisms such as adhesive interlayer plastic deformation). Moreover, their effect mainly depends on crack length and hexagonal size.

The interface that connects hexagonal tiles plays an essential role in enhancing the toughness of the architectured ceramics made of brittle constituents. In this study, the effect of weak interfaces on both strength and toughness using FE modeling and 3D DIC techniques was examined. The 3D network of weak interfaces ensures microcracks formation and crack deflection, leading to frictional energy dissipation as a major extrinsic toughening mechanism. Two types of crack propagation were distinguished, one with rapid propagation along an irregular path to the edges of the plain ceramic causing catastrophic failure, and the other one featuring a progressive propagation along predefined edges on the architectured ceramics, as demonstrated by DIC maps shown in Fig. 13.

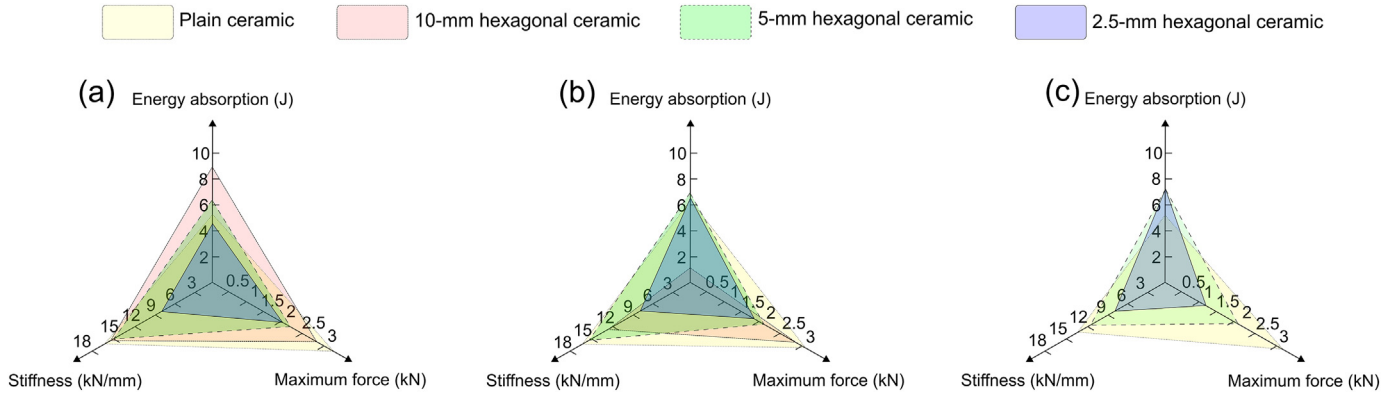

Fig. 12. Impact response of multilayered ceramics following three consecutive impacts: (a) First impact, (b) Second impact, and (c) Third impact.

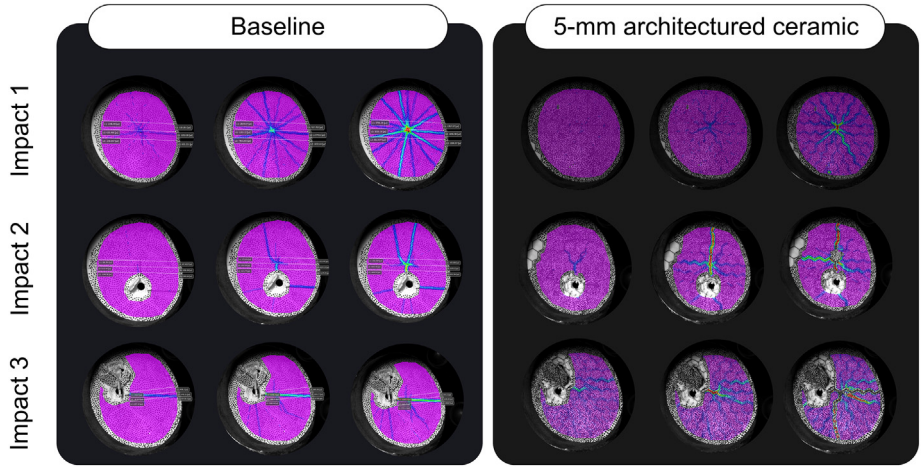

Fig. 13. DIC maps showing the crack propagation during the impact testing for the baseline and 5-mm hexagonal architectured ceramic.

By studying the crack propagation in the architectured ceramics, the important role of the adhesive interlayers was demonstrated, providing an intrinsic toughening mechanism, namely plastic deformation of the adhesive interlayers in a process zones underneath the 3D network of weak interfaces. The interlayers carried only shear loads due to their lower bending stiffness and strength compared to the ceramic layers. In addition, their high shear deformability facilitated near-uniform transfer of shear stress between the tiles, a phenomenon that provided more room to interact with the ceramic layers in the architectured ceramics due to their 3D network of ductile interfaces.

The energy absorption of architectured ceramics (U_c) can be expressed as [33]:

$$U_c = k\tau_i\gamma_i(1-\varphi) \tag{5}$$

where φ, τ_i and γ_i are the ceramic tile volume fraction, the failure stress and failure shear strain of the adhesive interlayers, respectively. Ceramic tile volume fraction, and the failure stress of the adhesive interlayers are the same for the baseline and architectured ceramics. As a result, an increase in the crack length, that is associated with delayed

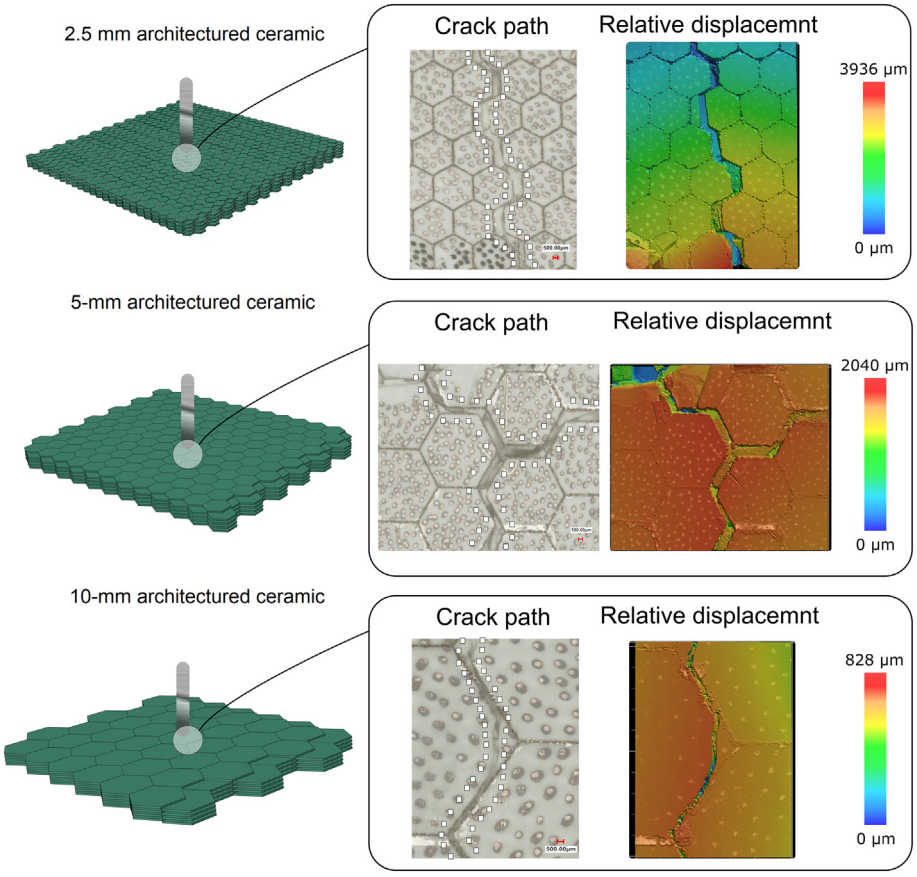

Fig. 14. Microscopic images showing the crack path on the surfaces of the 2.5-, 5- and 10-mm hexagonal architectured ceramics (the color bar represents the distance from the lowest point of cracks.).

shear failure of the adhesive interlayers (γ_i), can be an important factor contributing to the larger energy absorption of the architectured ceramics. There was a significant drop in the amount of plastic deformation of the adhesive interlayers in the plain ceramic system. The cracks propagated vertically throughout the cross section alongside a straight path, causing the plain ceramic to show a brittle fracture mode and unstable crack propagation. The length of the crack path was equal to the panel thickness. In contrast, the cracks grew within the weak interfaces of the architectured ceramics and were continually deflected when encountering a hexagonal tile as shown in Fig. 14. This phenomenon resulted in a zigzag pattern, which created a polyline path due to deflection and crack branching at the vertical interfaces. Based on FE analysis, the lengths of the crack path were 22%, 16% and 10% larger than the architectured panel's thickness for the 10-, 5-, and 2.5-mm hexagonal ceramics, respectively, which was not the case with the plain ceramic. Since the dissipated fracture energy primarily depends on the crack path length (see Eq. (5)), a larger amount of energy was dissipated in the architectured ceramics as compared to the baseline. Significant number of microcracks and crack deflection extrinsically promoted toughening in the architectured ceramics due to easier deviation of cracks via the weak interfaces, which is a key toughening structural feature. Alternatively, the plain ceramic showed brittle behaviour with little or no microcracking and limited crack deflection.

5. Summary

Natural materials show exceptional mechanical properties such as high toughness and stiffness, which are a result of their unique microstructure. Inspired by these complex features, a complete set of experimental and FE analyses were performed to engineer multilayered ceramics combing hard architectured layers with soft interfaces. The results established underlying mechanisms governing the toughness of the developed ceramics. Besides frictional dissipation, crack deflection and delamination were identified as the two major extrinsic mechanisms that significantly increase the crack path length inside the architectured ceramics, which led to a higher toughness. The developed computational model has demonstrated its ability to capture complex dynamic toughening mechanisms within the multilayered plain and architectured ceramics. The use of this comprehensive model can provide the potential to design a new class of architectured ceramics with high toughness and stiffness properties, a class of material with brittle constituents and 3D networks of ductile interfaces.

Declaration of Competing Interest

The authors declare that they have no known competing financial interests or personal relationships that could have appeared to influence the work reported in this paper.

The authors declare the following financial interests/personal relationships which may be considered as potential competing interests:

Acknowledgment

The work was funded by the security, materials, and technologies (SMT) program at National Research Council Canada (NRC). The authors acknowledge M. Mirkhalaf, R. Desnoyers, E. Poirier and F. Kirby for the scientific contributions, and the technical assistant for impact testing, laser processing and DIC.

References

[1] U.G. Wegst, H. Bai, E. Saiz, A.P. Tomsia, R.O. Ritchie, Bioinspired structural materials, Nat. Mater. 14 (1) (2015) 23–36.
[2] N.P. Padture, Advanced structural ceramics in aerospace propulsion, Nat. Mater. 15 (8) (2016) 804.
[3] R.B. Heimann, Classic and Advanced Ceramics: From Fundamentals to Applications, John Wiley & Sons, 2010.
[4] M.F. Ashby, D. Cebon, Materials selection in mechanical design, MRS Bull. 30 (12) (2005) 995.
[5] F. Barthelat, Architectured materials in engineering and biology: fabrication, structure, mechanics and performance, Int. Mater. Rev. 60 (8) (2015) 413–430.
[6] H. Yazdani Sarvestani, M. Mirkhalaf, A. Akbarzadeh, D. Backman, M. Genest, B. Ashrafi, Multilayered architectured ceramic panels with weak interfaces: energy absorption and multi-hit capabilities, Mater. Des. 167 (2019) 107627, https://doi.org/10.1016/j.matdes.2019.107627.
[7] H. Yazdani Sarvestani, C. Beausoleil, M. Genest, B. Ashrafi, Architectured ceramics with tunable toughness and stiffness, Extreme Mech. Lett. 39 (2020) 100844, https://doi.org/10.1016/j.eml.2020.100844.
[8] M.F. Ashby, Hybrids to fill holes in material property space, Philos. Mag. 85 (26–27) (2005) 3235–3257.
[9] B.E. Flammang, S. Alben, P.G. Madden, G.V. Lauder, Functional morphology of the fin rays of teleost fishes, J. Morphol. 274 (9) (2013) 1044–1059.
[10] P. Fratzl, O. Kolednik, F.D. Fischer, M.N. Dean, The mechanics of tessellations–bioinspired strategies for fracture resistance, Chem. Soc. Rev. 45 (2) (2016) 252–267.
[11] O. Bouaziz, Y. Bréchet, J.D. Embury, Heterogeneous and architectured materials: a possible strategy for design of structural materials, Adv. Eng. Mater. 10 (1–2) (2008) 24–36.
[12] M. Mirkhalaf, T. Zhou, F. Barthelat, Simultaneous improvements of strength and toughness in topologically interlocked ceramics, Proc. Natl. Acad. Sci. 115 (37, 2018) 9128–9133.
[13] H. Zhu, H. Cao, X. Liu, M. Wang, X. Meng, Q. Zhou, L. Xu, Nacre-like composite films with a conductive interconnected network consisting of graphene oxide, polyvinyl alcohol and single-walled carbon nanotubes, Mater. Des. 175 (2019) 107783.
[14] T. Magrini, F. Bouville, A. Lauria, H. Le Ferrand, T.P. Niebel, A.R. Studart, Transparent and tough bulk composites inspired by nacre, Nat. Commun. 10 (1) (2019) 1–10.
[15] M. Mirkhalaf, A. Sunesara, B. Ashrafi, F. Barthelat, Toughness by segmentation: fabrication, testing and micromechanics of architectured ceramic panels for impact applications, Int. J. Solids Struct. 158 (2019) 52–65.
[16] R. Wang, Z. Suo, A. Evans, N. Yao, I.A. Aksay, Deformation mechanisms in nacre, J. Mater. Res. 16 (9) (2001) 2485–2493.
[17] R.O. Ritchie, The conflicts between strength and toughness, Nat. Mater. 10 (11, 2011) 817–822.
[18] K. Radi, D. Jauffres, S. Deville, C.L. Martin, Strength and toughness trade-off optimization of nacre-like ceramic composites, Compos. Part B 183 (2020) 107699.
[19] F. Bouville, E. Maire, S. Meille, B. Van de Moortèle, A.J. Stevenson, S. Deville, Strong, tough and stiff bioinspired ceramics from brittle constituents, Nat. Mater. 13 (5) (2014) 508–514.
[20] S. Askarinejad, S. Youssefian, N. Rahbar, Toughening and strengthening mechanisms in bamboo from atoms to fibers, Handb. Mater. Model.: Appl.: Curr. Emerg. Mater. (2020) 1597–1625.
[21] L.J. Gibson, The hierarchical structure and mechanics of plant materials, J. R. Soc. Interface 9 (76) (2012) 2749–2766.
[22] M.A. Meyers, J. McKittrick, P.-Y. Chen, Structural biological materials: critical mechanics-materials connections, Science 339 (6121) (2013) 773–779.
[23] L.S. Dimas, G.H. Bratzel, I. Eylon, M.J. Buehler, Tough composites inspired by mineralized natural materials: computation, 3D printing, and testing, Adv. Funct. Mater. 23 (36, 2013) 4629–4638.
[24] A.S. Dalaq, F. Barthelat, Manipulating the geometry of architectured beams for maximum toughness and strength, Mater. Des. (2020) 108889.
[25] N. Abid, F. Hannard, J. William Pro, F. Barthelat, Exploring the fracture toughness of tessellated materials with the discrete-element method, J. Appl. Mech. 86 (11) (2019).
[26] M. Mirkhalaf, A. Sunesara, B. Ashrafi, F. Barthelat, Toughness by segmentation: Fabrication, testing and micromechanics of architectured ceramic panels for impact applications, Int. J. Solids Struct. 158 (2019) 52–65.
[27] C. Beausoleil, H. Yazdani Sarvestani, Z. Katz, J. Gholipour, B. Ashrafi, Deep and high precision cutting of alumina ceramics by picosecond laser, Ceram. Int. 46 (10, Part A) (2020) 15285–15296, https://doi.org/10.1016/j.ceramint.2020.03.069.
[28] I. Esmail, H. Yazdani Sarvestani, J. Gholipour, B. Ashrafi, Engineered net shaping of alumina ceramics using picosecond laser, Opt. Laser Technol. 135 (2021) 106669, https://doi.org/10.1016/j.optlastec.2020.106669.
[29] Z. Yin, A. Dastjerdi, F. Barthelat, Tough and deformable glasses with bioinspired cross-ply architectures, Acta Biomater. 75 (2018) 439–450.
[30] A. Standard, D3763-06 Standard test method for high speed puncture properties of plastics using load and displacement sensors, ASTM Intern. (2006) (D20 Plastics D 20).
[31] G.R. Johnson, T.J. Holmquist, An Improved Computational Constitutive Model for Brittle Materials, AIP Conference ProceedingsAmerican Institute of Physics 1994, pp. 981–984.
[32] D. Liu, H. Zhu, C. Huang, J. Wang, P. Yao, Prediction model of depth of penetration for alumina ceramics turned by abrasive waterjet—finite element method and experimental study, Int. J. Adv. Manuf. Technol. 87 (9–12) (2016) 2673–2682.
[33] F. Barthelat, Designing nacre-like materials for simultaneous stiffness, strength and toughness: optimum materials, composition, microstructure and size, J. Mech. Phys. Solids 73 (2014) 22–37.